geosciences

MDPI

Article

Spatial Prediction of Future Flood Risk: An Approach to the Effects of Climate Change

Mohammadtaghi Avand [1,*], Hamid Reza Moradi [1] and Mehdi Ramazanzadeh Lasboyee [2]

[1] Department of Watershed Management Engineering, College of Natural Resources and Marine Science, Tarbiat Modares University, Noor 46414-356, Iran; hrmoradi@modares.ac.ir
[2] Department of Tourism Management, College of Humanities & Social Sciences, Mazandaran University, Babolsar 47416-13534, Iran; M.ramazanzadeh@umz.ac.ir
* Correspondence: mt.avand@modares.ac.ir

Abstract: Preparation of a flood probability map serves as the first step in a flood management program. This research develops a probability flood map for floods resulting from climate change in the future. Two models of Flexible Discrimination Analysis (FDA) and Artificial Neural Network (ANN) were used. Two optimistic (RCP2.6) and pessimistic (RCP8.5) climate change scenarios were considered for mapping future rainfall. Moreover, to produce probability flood occurrence maps, 263 locations of past flood events were used as dependent variables. The number of 13 factors conditioning floods was taken as independent variables in modeling. Of the total 263 flood locations, 80% (210 locations) and 20% (53 locations) were considered model training and validation. The Receiver Operating Characteristic (ROC) curve and other statistical criteria were used to validate the models. Based on assessments of the validated models, FDA, with a ROC-AUC = 0.918, standard error (SE = 0.038), and an accuracy of 0.86% compared to the ANN model with a ROC-AUC = 0.897, has the highest accuracy in preparing the flood probability map in the study area. The modeling results also showed that the factors of distance from the River, altitude, slope, and rainfall have the greatest impact on floods in the study area. Both models' future flood susceptibility maps showed that the highest area is related to the very low class. The lowest area is related to the high class.

Keywords: flood hazard; climate change; data mining model; ROC curve

Citation: Avand, M.; Moradi, H.R.; Ramazanzadeh Lasboyee, M. Spatial Prediction of Future Flood Risk: An Approach to the Effects of Climate Change. *Geosciences* **2021**, *11*, 25. https://doi.org/10.3390/geosciences11010025

Received: 22 November 2020
Accepted: 31 December 2020
Published: 5 January 2021

1. Introduction

Since the beginning of the second half of the nineteenth century, significant climate changes have taken place. These, in turn, have led to widespread shifts in rainfall regimes, pressure patterns, and sea surface temperatures, resulting in the direct and indirect effects on various aspects of life on earth [1]. Among the most significant effect was the rising global temperature. According to several studies conducted on different parts of the world, significant temporal and spatial changes in precipitation and evaporation occurred upon the earth's rising temperature. Altogether, such changes in rainfall patterns cause water resources have changed [2,3].

According to the IPCC reports, climate change has caused hydrological changes worldwide in recent years, increasing the possibility of extreme weather events such as floods [4]. Due to the adaptation of human societies' ecosystems and physical structures to normal climatic conditions, they do not have sufficient resilience under extreme climatic phenomena. Therefore, such anomalies can adversely affect ecosystems and communities and cause significant economic and social damage [1,5].

Global warming increases the magnitude and frequency of maximum rainfall. This subsequently leads to severe and broader floods in flooded rivers. Studies show that the frequency of floods varies depending on local climate and the watershed characteristics in different parts of the world [6,7]. Uncertainty about climate change's effects on severe

events is challenging at both the local and regional levels. To reduce the risk of flooding, it is necessary to identify the flood-prone area in current and future environmental conditions [8–10]. Different models can be used to prepare a flood probability map after heavy rain or storm (danger) to assess the risk [11]. The most important models and methods used in the preparation of climate change-related flood risk mapping include hydrological models [12–14], statistical models [15,16], and GIS [17–21].

Recently, given the importance of climate change and its impacts on increasing runoff and the number of floods in different parts of the world, literature is fraught with studies using different models and approaches in this field [22–24]. The following are some critical studies on the impacts of climate change on floods:

Rutger Dankers and Luc Feyen assessed the effects of climate change and the risk of catastrophic floods in Europe. They found that maximum discharge levels are probably observed in many European rivers (both in scale and frequency) by the end of this century. Moreover, in some rivers, especially those located in western and parts of Eastern Europe, the return period of floods was reduced. However, a significant reduction in the risk of floods in the northeastern parts is predicted. Due to warmer winter in these areas, shorter snowfall seasons can significantly reduce snowmelt in spring. Simultaneously, other rivers in central and southern Europe are characterized by a significant reduction in peak discharge [25].

In a study to prepare a flood susceptibility map in the Tessta River in northern Bangladesh, two-hybrid model groups, including Dagging, Random Subspace (RS), Artificial Neural Network (ANN), Random Forest (RF), and Support Vector Machine (SVM) were used. Moreover, 12 factors affecting the flood and 413 current and former flood locations were used. A multi-line detection test was used to determine the relationship between flood occurrence and factors affecting flood. To validate and compare the models, Wilcoxon, Friedman, paired t-test, and Relative Characteristic Curve (ROC) were used. The Area Under the ROC (AUC) value indicated that the Dagging model was more accurate than the other models [26].

The impact of climate change on flooding and humans in the Deba River Basin (northern Spain) was studied by [27]. In this study, four RCM models and the MIKESHE-MIKE11 hydrological model were used. The results showed that the maximum discharge with a return period of 40 years for the three models between 14 and 15 percent in 2001–2040. Moreover, for two models in 2041–2080, this increase between 14 and 19 percent was recorded. Moreover, it was forecasted that flood areas and the severity of its risks would increase.

The Ajoy River in eastern India faces severe flooding during monsoon rains. This region has a large population and good agricultural productivity. The current study maps flood prone-areas in the Ajoy River Basin using Support Vector Machine (SVM), Random Forest (RF), and Biogeography-Based Optimization (BBO). Various factors affecting floods (topography, hydrology, soil characteristics, environment, and geology) were considered. The results of these models were evaluated using the area under the ROC curve (AUC). The AUC values for BBO, RF, and SVM are 0.985, 0.925, and 0.896, respectively. Therefore, the BBO model (AUC = 0.98) had the highest accuracy and showed that BBO is a prominent method for identifying flood-prone areas in eastern India [28].

The literature review showed that given the importance of climate change and floods, different methods and models had been used to evaluate them. Pros and cons characterize each one. Recently, new machine learning methods in hydrological [29–32] and climate modeling [33,34] have been widely applied. However, machine learning methods have rarely been used to investigate climate change's effect on flood susceptibility areas.

In this study, flood-prone area due to the existence of extensive agricultural lands, especially rice cultivation around the Tajan River, and the role of agriculture in the economy of the people of this basin, was determined. Therefore, the most important objectives of this study include: 1—Determining the areas with flood probability risk in the current and future 2—Selecting the most important factors affecting the flood in the study area 3—Evaluating two machine learning methods. For this, two data mining models of artificial

neural network (ANN) and flexible discriminant analysis (FDA) under two optimistic (RCP2.6) and pessimistic (RCP8.5) climate scenarios were used. This approach has rarely been used in mapping future flood probability. Therefore, it is necessary to evaluate this approach using data mining models.

2. Materials and Methods

2.1. Description of the Study Area

Tajan watershed, with approximately area 4000 Km^2 is located in Mazandaran province and the southern part of Sari city. The study area between longitude 53°18′ to 53°05′ and latitude 36°29′ to 36°09′ is located. This basin is surrounded on one side by the Caspian Sea and the other by the Alborz Mountains. Part of the study basin is located in the elevations of Semnan province and part in the highlands of Neka city (Figure 1). The average annual temperature of this area is approximately 15 °C, and the amount of annual rainfall is 832 mm [35]. Tajan watershed's topography varies from −2 m at the watershed outlet to 3670 m above sea level (asl). The most important rivers in this region are Tajan and Zaremrud rivers. Forestlands cover the largest area of this region, followed by irrigated agricultural and dry farming lands. The primary agricultural land use in the downstream areas up to the middle parts of this watershed is rice planting. Due to topographic conditions and lack of sufficient water resources, dry farming crops are grown at higher altitudes. The main occupation of most people in this area is agriculture. The occurrence of floods in this area will significantly damage their agriculture and increase their vulnerability and reduce their resilience to other natural hazards.

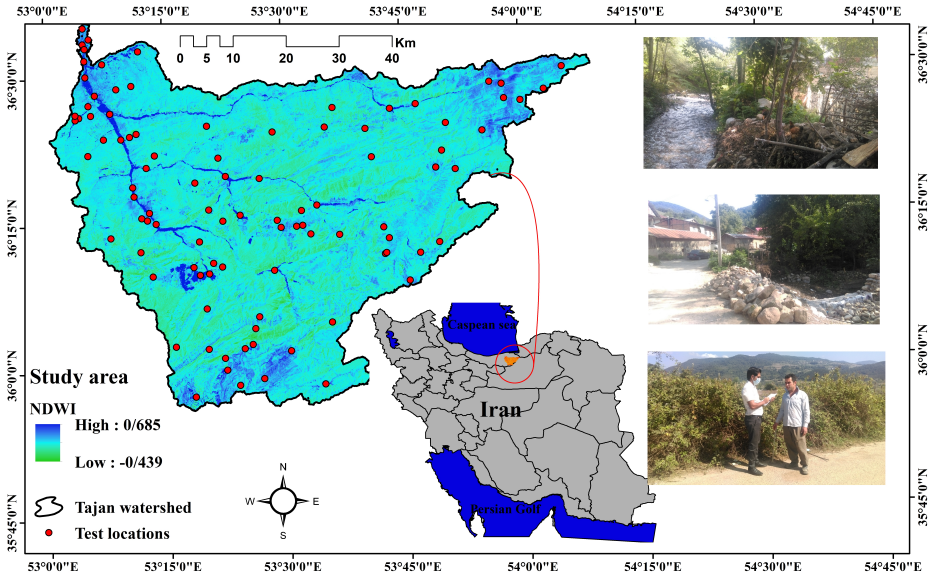

Figure 1. Location of the study area in Iran.

2.2. Methods

2.2.1. Flood Inventory Map

Zonation of floods that have occurred in the past is necessary to predict future floods. The reasons are that there is a strong correlation between them [36–38]. Therefore, first, using various methods, including reviewing maps and photos of previous floods, field surveys, and using Google Earth, previous flood areas were identified. Then, a flood susceptibility map was prepared. In this research, a flood map is considered a binary classification in which flood inventory is converted into two classes of flood locations (1) and non-flood locations (0). Therefore, to prepare a list of flood training inventory that is a dependent variable, flood points (points 1) and non-flood points (points 0) are needed. Flood points indicate areas where floods have occurred in the past decade, and non-flood points indicate areas where no floods have been recorded in the past decade. Flood and

non-flood zones were prepared in polygons, which were first turned into points and then into modeling. Finally, 263 flood points and 263 flood non-flood points were identified. These points were divided into two categories for modeling: 80% (212) for training and 20% (53) for validation. Finally, in this study, R software version 3.3 was used to prepare a flood probability map of the study area (Figure 2).

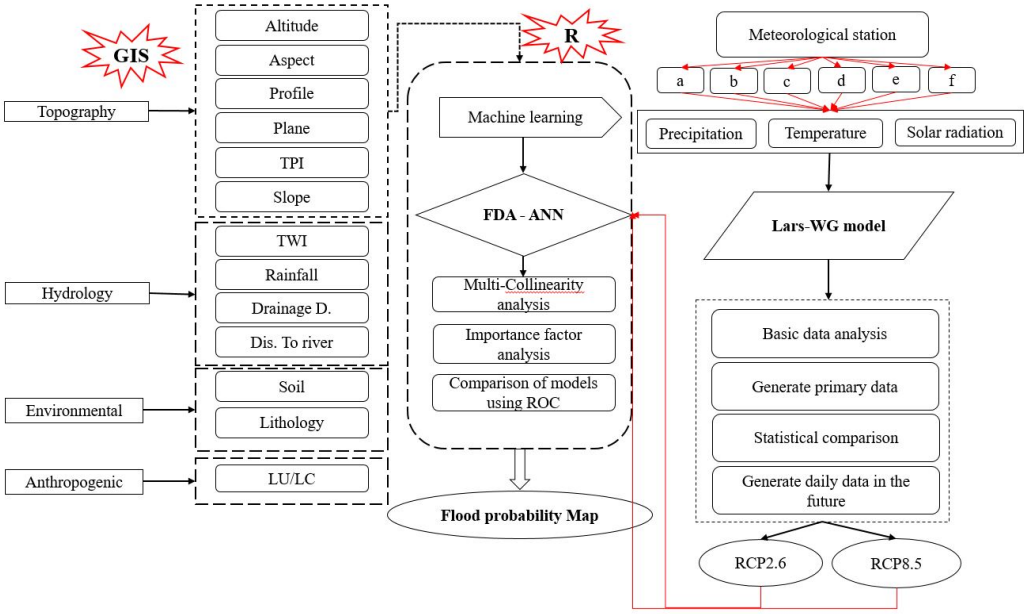

Figure 2. Research flow chart.

2.2.2. Flood Conditioning Factors

Flood susceptibility mapping is a complex process. It depends on many factors, such as topographic, hydrological, geomorphological, and climatic factors [38,39]. Therefore, to prepare a flood probability map of an area, it is necessary to determine the critical and practical factors of floods. Literature review [40,41] showed that the most critical factors affect floods. They include altitude, slope, slope aspect, rainfall, land use, plan curvature, plan curvature, distance from the River, drainage density, lithology, soil, topographic wetness index (TWI), and terrain position index (TPI) (Figure 2). In this study, these 13 factors were selected as independent variables affecting the flood. They were prepared using Arc Map software version 10.4.1 (Esri, Redlands, CA, USA) and Saga 3.3-version (SAGA, Hamburg, Germany) (Figure 2). The base layer for preparing some of these layers was a digital elevation models (DEM) with a spatial resolution of 12.5 m, downloaded from the https://vertex.daac.asf.alaska.edu/ site. The importance of each of these layers on flooding is explained below.

Topographical Conditioning Factors

The most critical factors affecting runoff in a watershed are topographic factors [42–44]. Elevation, slope, and aspect in an area can cause severe hydrological changes in the watershed by changing the velocity and volume of runoff [45]. For example, steep areas increase the rate of runoff evacuation and reduce runoff accumulation in the area. Areas with lower elevation and slopes increase the runoff height and flooding of the area. The slope aspect could also affect the runoff amount due to its effect on soil moisture [46,47]. For example, in the northern hemisphere, the northern and western aspects have less permeability due to more moisture. Moreover, the potential for runoff production in these areas is greater than the southern and eastern ones. In this research, slope, aspect, and altitude maps were prepared using a digital elevation model with a spatial resolution of 12.5 m in the GIS software (Figure 3).

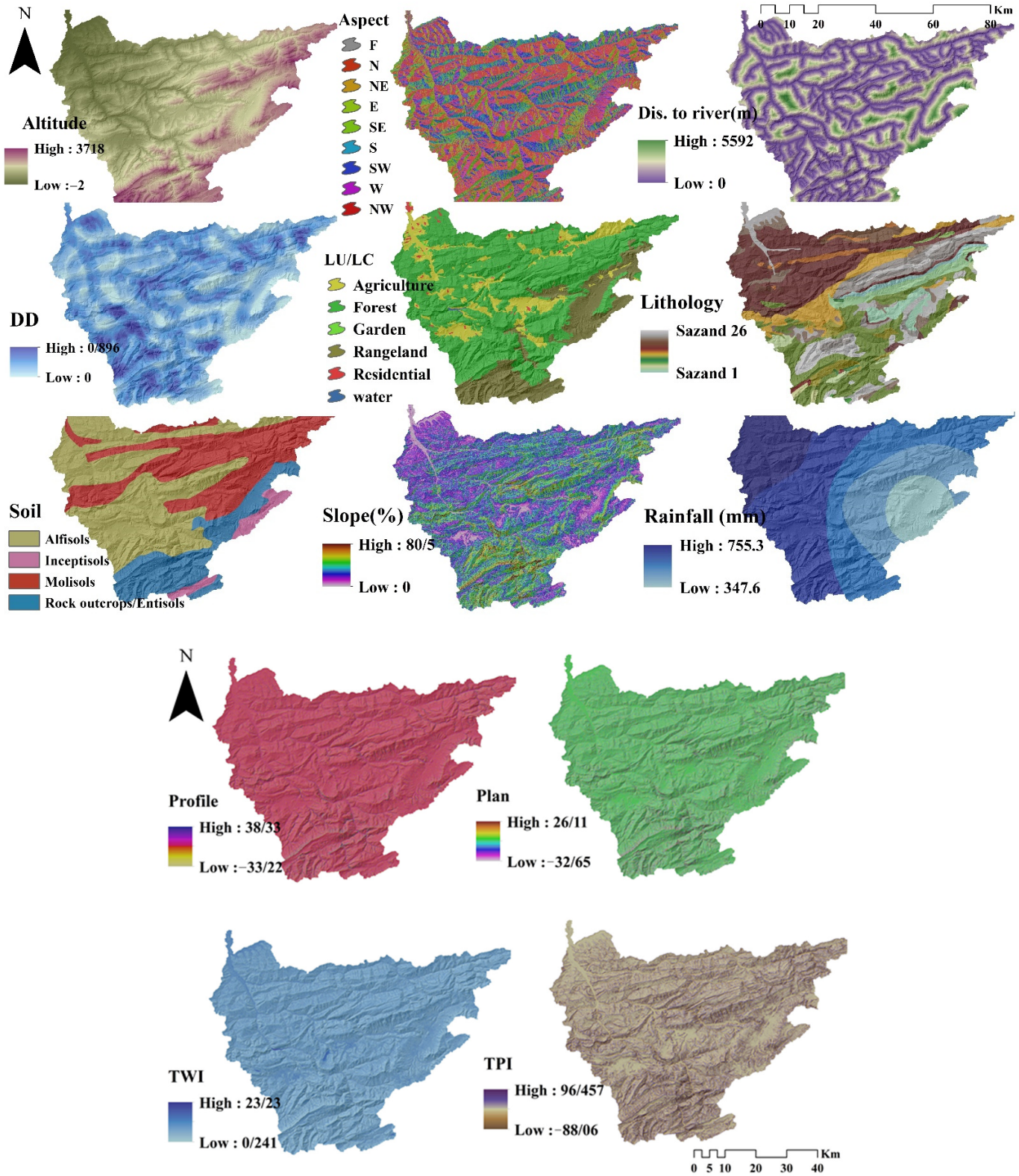

Figure 3. Flood-conditioning factors of the study area.

As curvature is useful in the water budget, it has been used in preparing the flood susceptibility map [48]. The curvature of the profile indicates the change in slope along the flow line and rotation rate. The curvature of the plane indicates the change in direction along a meter. It shows the convergence of flow and deviation [36]. The plan and profile

curvature are divided into three classes: concave, convex, and flat. These two layers were prepared using a DEM map in ASCII format in the Saga software environment (Figure 3).

Hydrological Conditioning Factors

The most critical factor affecting flood damage is the distance from the River. For this reason, this layer is used in most flood-zoning studies. The distance from the River is inversely related to the amount of damage caused by the flood [26,37]. This layer was prepared using the layer of rivers in the watershed and the GIS software distance tool. The Drainage Density (DD) layer also is vital in flood susceptibility mapping. This is due to its effect on the expansion and discharge of runoff from the floodplain area. This layer was also prepared using the river layer and the Density tool in GIS software (Figure 3).

The topographic wetness index also affects the flood of an area. This index shows the amount of water stored per pixel in the study area. Floods are more common in areas with high topographic humidity [48]. The amount of water stored in each pixel is obtained using the following equation.

$$TWI = \frac{\ln(A_s)}{\tan\beta} \quad (1)$$

where, A_s indicates the specific catchment area (m^2m^{-1}), and $\tan\beta$ indicate slopes of the basin in degrees. This layer was obtained in the Saga software environment using the DEM map (Figure 3).

Rainfall is found to be the most crucial trigger for floods in a region. This factor affects the volume and intensity of floods in an area. The amount of rainfall in each region depends on its topographic and climatic conditions [49,50]. To prepare the rainfall layer in this research, annual rainfall data of 6 (Sangdeh, Soleaman tangeh, Kordkhil, Kiasar, Qarakhil, Rig cheshmeh) stations with a period of 25 years (1990–2015) have been used. Due to its greater accuracy than the IDW method, the Kriging interpolation method was selected to produce the final rainfall map (Figure 3).

Environmental Conditioning Factors

Land use the most critical factor affecting surface runoff and the amount of sediment and, consequently, the flood in an area [18]. Because land use directly affects surface runoff and infiltration rate. For this reason, the number of floods increases in residential areas due to the increase in the area of impervious lands. Therefore, the occurrence of floods is inversely related to vegetation density [38]. In this study, to prepare the land use layer in 2019, Landsat satellite images and sensor OLI were used. This image was used after geometric and atmospheric corrections and its validation with training samples in ENVI software 5.3-version (Harris Geospatial, Broomfield, CO, USA) (Figure 3).

The type of lithological formation also plays an essential role in flooding. Areas with permeable soils and hard lithological formations are characterized by lower waterway density [19]. The lithological layer in this study was prepared using the Iranian lithological layer with a scale of 1/50,000. It has 25 types of lithological formations (Table 1, Figure 3). The type and texture of the soil in the study area also affect the volume of runoff. In areas with higher soil depth and permeability, the surface runoff amount is reduced (Figure 3). In this study, the study area's soil map was obtained from the Natural Resources Department of Mazandaran province at a scale of 1/100,000.

Table 1. Characteristics of existing formations in the study area.

Number	Code	Description	Age
1	Cm	Dark grey to black fossiliferous limestone with subordinate black shale (MOBARAK FM)	Carboniferous
2	Dbsh	Undifferentiated limestone, shale, and marl	Devonian
3	Dj	Yellowish, thin to thick-bedded, fossiliferous argillaceous limestone, dark grey limestone, greenish marl, and shale, locally including gypsum	Devonian
4	E	Nummulitic limestone	Eocene
5	E1	Dark red medium-grained arkosic to subarkosic sandstone and micaceous siltstone (LALUN FM)	Cambrian
6	E2l2	Globotruncа limestone	Late.Cretaceous
7	Ebt	Alternation of dolomite, limestone, and variegated shale (BARUT FM)	Cambrian
8	Em	Dolomite platy and flaggy limestone containing trilobite; sandstone and shale (MILA FM)	Cambrian
9	Ez	Reef-type limestone and gypsiferous marl (ZIARAT FM)	Paleocene-Eocene
10	J	Light grey, thin-bedded to massive limestone (LAR FM)	Jurassic-Cretaceous
11	K1l	Thick bedded to massive, white to pinkish orbitolina bearing limestone (TIZKUH FM)	Early.Cretaceous
12	K2	Hyporite bearing limestone (Senonian)	Late.Cretaceous
13	K2plm	Thick-bedded to massive limestone (maastrichtian)	Late.Cretaceous
14	Mc	Red conglomerate and sandstone	Miocene
15	Msm	Marl, calcareous sandstone, sandy limestone, and minor conglomerate	Miocene
16	Pd	Red sandstone and shale with subordinate sandy limestone (DORUD FM)	Permian
17	Pec	Light-red coarse-grained, a polygenic conglomerate with sandstone intercalations	Paleocene-Eocene
18	PEk	Dull green grey slaty shales with subordinate intercalation of quartzitic sandstone (KAHAR FM; Morad series and Kalmard Fm)	Pre-Cambrian
19	Pel	Medium to thick-bedded limestone	Paleocene-Eocene
20	PEm	Marl and gypsiferous marl locally gypsiferous mudstone	Paleocene-Eocene
21	Plc	Polymictic conglomerate and sandstone	Pliocene
22	Pr	Dark grey medium-bedded to massive limestone (RUTEH LIMESTONE)	Permian
23	Qt	High-level piedmont fan and valley terrace deposits	Quaternary
24	TRe	Thin bedded, yellow to pinkish argillaceous limestone with worm tracks	Triassic
25	URig	Red marl, gypsiferous marl, sandstone, and conglomerate (Upper red Fm.)	Miocene

2.3. Description of the Data Mining Model

2.3.1. Flexible Discrimination Analysis (FDA)

FDA model is one of the non-parametric models for creating complex decision boundaries. This classification model is based on non-parametric regression models. It changes the response variable using optimal scoring to prepare the data better for linear separation [51,52]. The purpose of the FDA model is to modify the linear regression method by a parametric semi-regression method. This, in turn, creates a practical structure for various regression methods. FDA provides different discrimination rules (i.e., based on the relationships between flood occurrence and the predictor factors) and flexible class boundaries. FDA could create a predictive map that division the reduced space into subareas; they are identified with group membership, and the decision boundary type is linear [51,53]. The statistical background of this model is accurately stated in some studies [51,54].

An example of an FDA model extension is as follows:

$$\hat{Y} = S_x(Y) \quad (2)$$

where Y is an indicator response matrix and S_x is a regression procedure (Linear regression, Polynomial Regression, Additive Models, MARS, Neural Network ...).

The most important limitations of the LED method that led to the use of the LED method in this study are:

- Lots of data, many predictors: LDA under fits (restricts to linear boundaries)
- Many correlated predictors: LDA (noisy/wiggly coefficients)
- Dimension reduction limited by the number of classes

2.3.2. Artificial Neural Network (ANN)

An artificial neural network inspired by biological neural systems comprises several processing elements that usually operate in parallel. They are formed in regular architectures. An artificial neural network can learn, summons, and generalize data learning patterns [55]. The general structure of neural network models consists of three layers: the first layer is the input layer in which the input information is introduced to the model; the second layer is the hidden layer (s) in which the information is processed; the output layer is the third layer in which the results of the model performance are generated. Generally, neural networks are classified into supervised and unsupervised groups. In unsupervised training, neural network parameters are regulated by the system. However, in supervised training, a set of data and results or related responses are presented to the neural network [56].

Input data in the monitored type include training, experimental, and validation data. Training data are used to obtain optimal weights. Then, test data are entered into the system to obtain network error and efficiency. Validation data is used to prevent the model's false and over-modeling, which usually reduces the formal learning of the model's process. This data is a criterion for evaluating the performance of models [57].

One of the neural network algorithms used to solve the classification problem is LVQ. The LVQ network is a vector learning algorithm of a hybrid network that is trained in both supervised and unsupervised methods. This network has two layers, with each neuron in the first layer classifying a portion of the input based on the initial vector learning. Sometimes several neurons are given to a class and then in the second layer there is one neuron for each class. The second layer of LVQ is used to combine subclasses into a single network class. It is assumed that an optimal learning rule for the LVQ network must provide the differential equation from Equation (2) in the continuous space.

$$\frac{dm_i}{dt} = a_t u_i(x)(x - m_i) \tag{3}$$

Or in discrete space

$$\Delta m_i = a_t u_t(x)(x - m_i) \tag{4}$$

In relation 3, x is the input vector, mi is the neuron memory vector i. $u_i(x)$ is the output value of the neuron i where x is the input layer.

2.4. Predicting Climate Change

To investigate climate change's effect as an essential parameter, six synoptic and climatological stations of Sangdeh, Kordkhil, Kiasar, Qarakhil, Rig Cheshmeh, Soleaman tangeh in a statistical period of 25 years (1990–2015) were used. Three steps were performed to implement the Lars-WG model: First, to analyze the model and examine the observational data characteristics, the Site Analysis function was used in the Lars-WG model. In the next step, the observational data and the generated data were evaluated using the model to evaluate the model's ability to predict future data. Finally, climate change prediction was performed using Model HadESM2. Its outputs were created as two separate files containing RCP2.6 and RCP8.5 scenario data. After generating future climate data, the annual average rainfall for each station was calculated. A future rainfall map for different climatic scenarios was generated using the Kriging interpolation method in the GIS environment.

These layers were entered into data mining models as an independent variable to prepare a flood susceptibility map.

2.5. Receiver Operating Characteristic (ROC)

One of the appropriate methods to evaluate a classifier's results and evaluate its capability in identifying the desired class is to use the receiver operating characteristic (ROC) curve. It is used to evaluate the sensitivity of the method [58,59]. The sensitivity index refers to the relationship between the numbers of cells that are correctly classified. Then, the number of cells that are incorrectly classified. The greater the deviation from the baseline for a specific class in the ROC curve, the greater the classifier's efficiency in identifying that class. In addition to examining the desired class diagram trend, the area under the curve (AUC) is also calculated. The AUC indicates the probability of correctly classifying a randomly selected cell. This value indicates the reliability of the method [60–62].

In this index, the evaluation of cells that are correctly assigned to the desired class (TP), cells that are not correctly assigned to the desired class (TN), cells that are incorrectly assigned to the desired class (FP), and cells that are not incorrectly assigned to the desired class (FN) are considered [63,64]. To draw this curve, the x-axis, which represents the "1-Specificity", and the y-axis, which contains "sensitivity," calculated for each value of the desired class threshold.

$$Specificity = \frac{TN}{TN + FP} \quad (5)$$

$$Sensitivity = \frac{TP}{TP + FN} \quad (6)$$

To evaluate the results obtained by the models used, other statistical criteria including Bias, accuracy, True Skill Statistic (TSS), Cohen's Kappa (KAPPA), confidence interval (CI), success ratio (SR), and the probability of detection (POD) were also used.

3. Results

3.1. Project Climate Change

Climate change modeling results for the next 30 years (2020–2050) showed that rainfall changes would be significant in almost all stations. These results also show that the amount of rainfall in the RCP2.6 scenario in most months, especially in winter, is more than the RCP8.5 scenario. It seems that the number of rainfalls increases in all stations. Still, this increase is more in stations near the Caspian Sea, such as Kordkhil and Qarakhil, than stations at higher altitudes, such as Kiasar and Sangdeh (Figure 4).

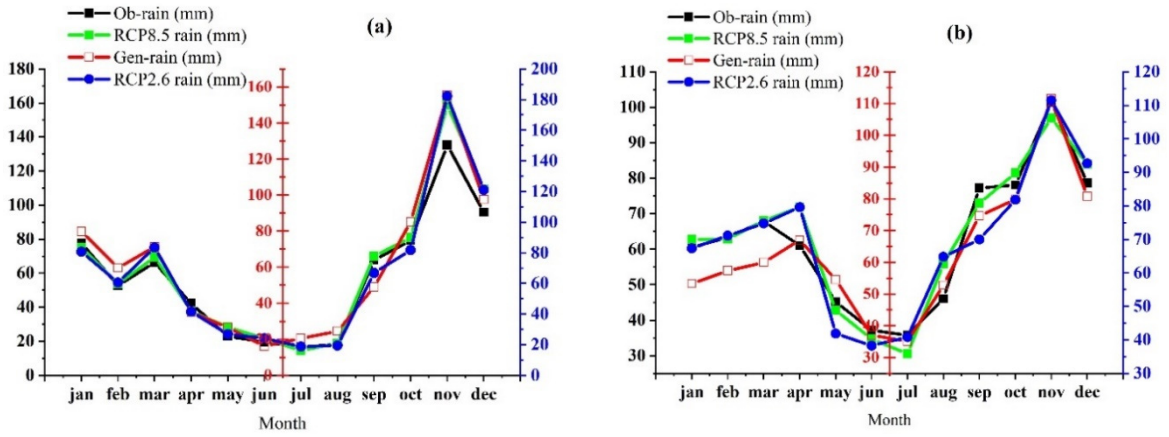

Figure 4. *Cont.*

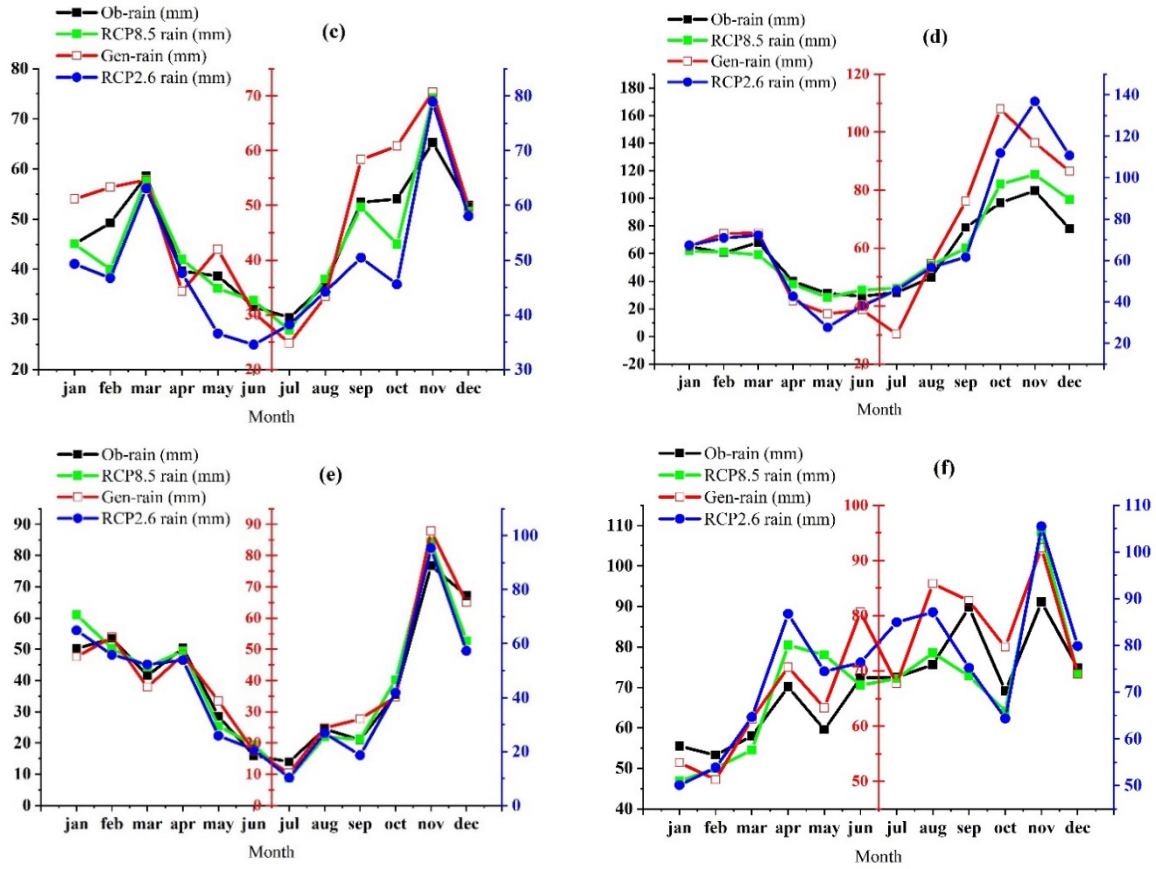

Figure 4. Rainfall data trends of the studied stations (**a**) Kordkhil (**b**) Rig cheshmeh (**c**) Solaman tangeh (**d**) Gharakhil (**e**) Kiasar (**f**) Sangdeh (Ob = observed and Gen = generated prediction).

3.2. The Importance of Influencing Factors

The results of floods factor analysis in the study area showed that in the ANN model, the distance from the River (43%), slope (21%), altitude (17%), and rainfall (9%) factors are the most important, respectively. While in the FDA model, distance from the River (45%), altitude (39%), slope (31%), land use (15%), and rainfall (14%) have the most significant impact on flood occurrence in the study area, respectively (Figure 5).

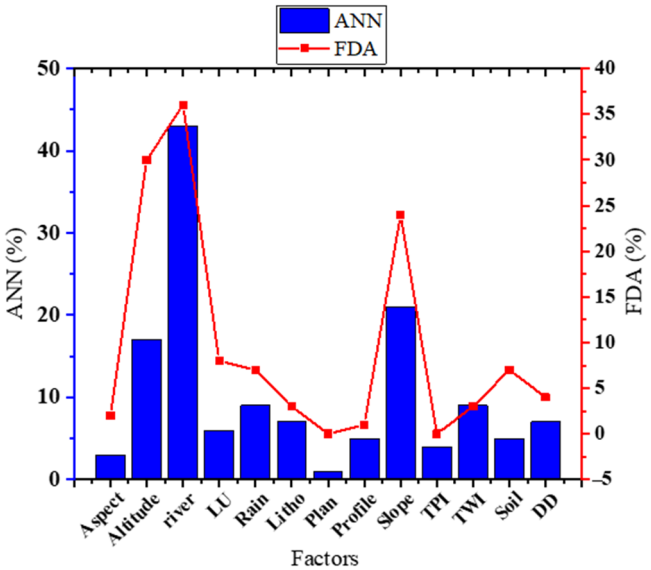

Figure 5. The relative importance of flood affecting factors using two ANN and FDA models.

The study area's flood susceptibility was mapped by two data mining models of ANN and FDA and two scenarios RCP2.6 and RCP8.5, then using natural break algorithm in a GIS software environment to 5 classes including very low, low, moderate, high and very high were classified. There are various algorithms in a GIS software for classifying raster map classes. They include natural break, equal interval, quintile, regular interval, standard deviation, and manual technique. The natural break algorithm is the most famous algorithm for classifying maps used in most studies. The flood susceptibility map of the models used is shown in Figures 6–8.

The flood classification area results using two models of ANN and FDA showed that under the influence of different climatic scenarios (RCP2.6 and RCP8.5), different parts of the watershed understudied are affected by floods. These results showed that 381 Km^2 (16%) and 352 Km^2 (15%) of the study area were identified by the FDA and ANN models as very high susceptibility classes, respectively. Moreover, In the ANN model under scenario RCP2.6, the flood susceptibility map class area includes very high, high, moderate, low, and very low, respectively 485, 226, 289, 1361, and 1555 Km^2, and under scenario RCP8.5, the flood susceptibility map classes area includes very high, high, moderate, low and very low, respectively 406, 204, 278, 586 and 2442 Km^2 (Figure 9).

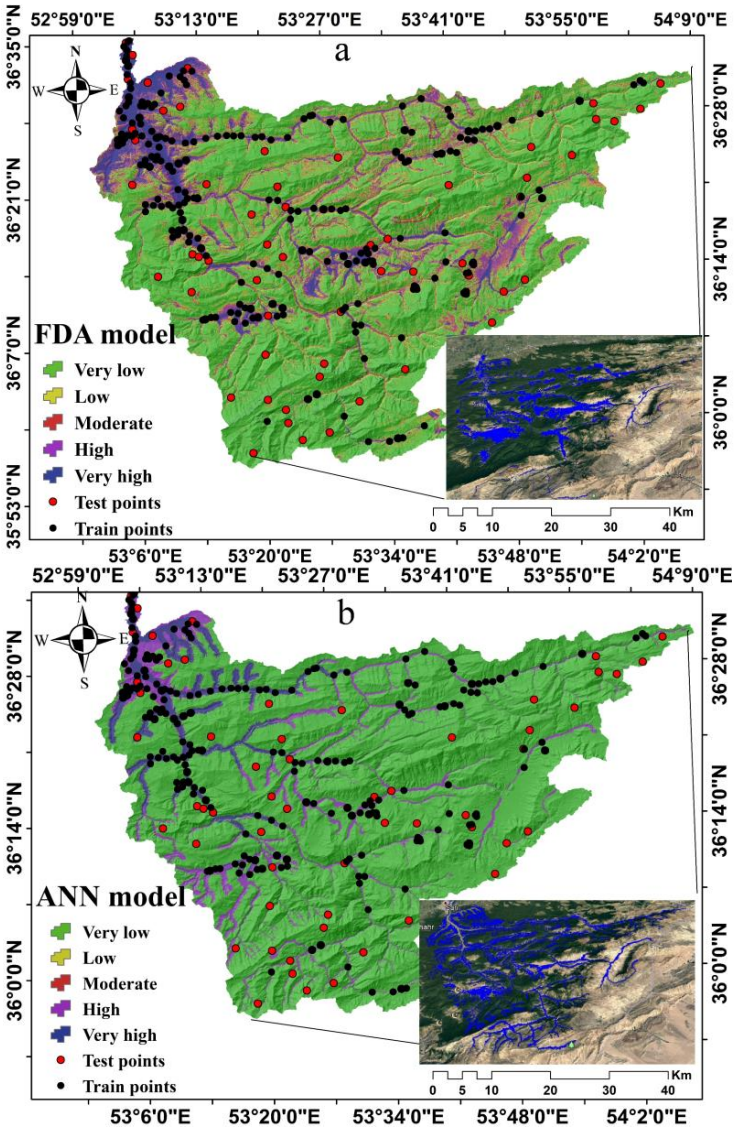

Figure 6. Flood susceptibility map: (**a**)—FDA model, (**b**)—ANN model.

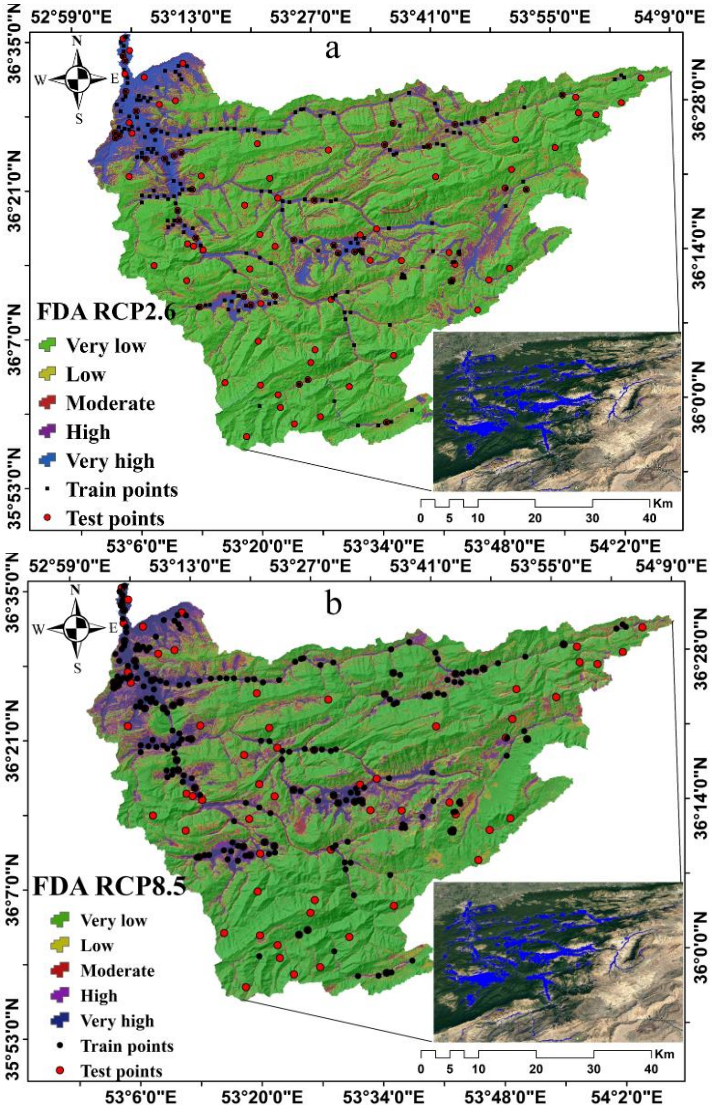

Figure 7. Flood susceptibility map prepared using FDA model (**a**)—RCP2.6, (**b**)—RCP8.5.

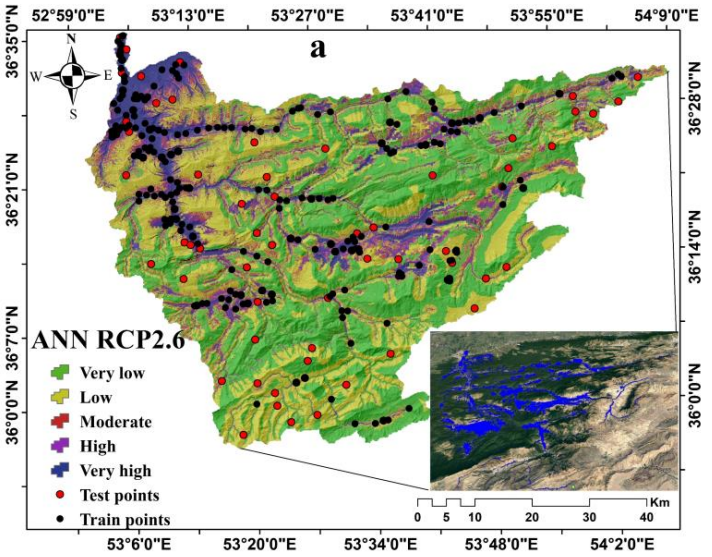

Figure 8. *Cont.*

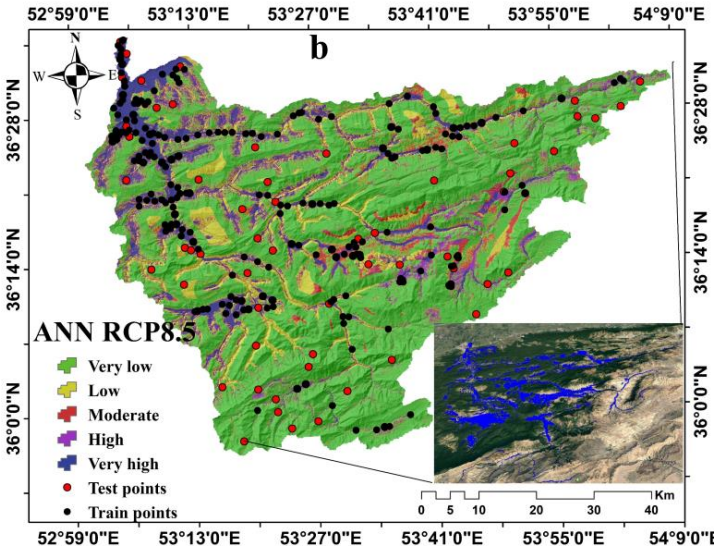

Figure 8. Flood susceptibility map prepared using ANN model (**a**)—RCP2.6, (**b**)—RCP8.5.

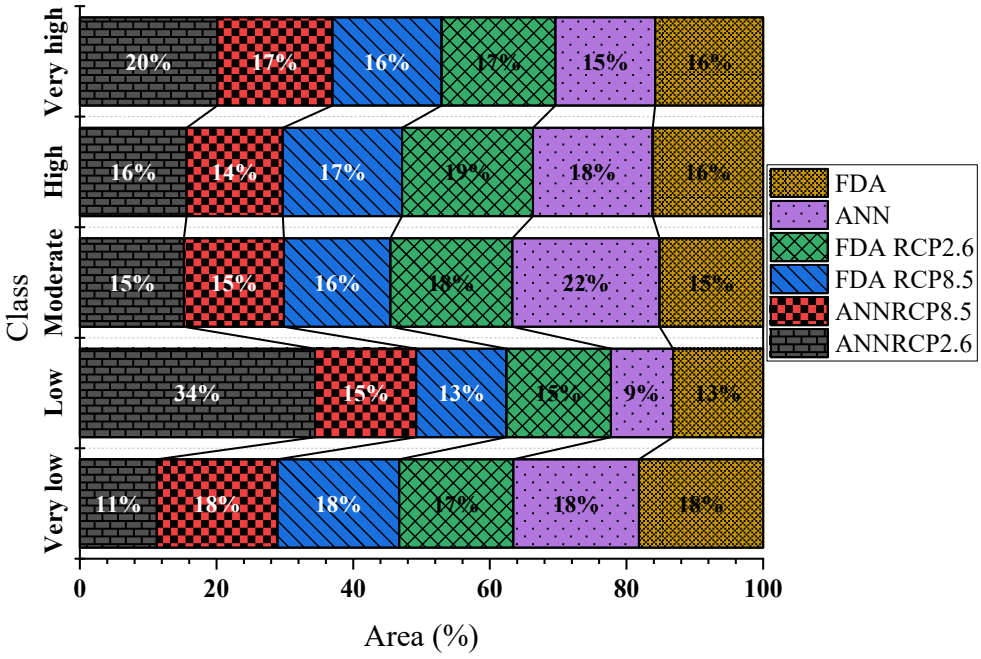

Figure 9. Area (Km^2) of flood susceptibility classes affected by two scenarios RCP2.6 and RCP8.5.

In the FDA model under scenario RCP2.6, the flood susceptibility map classes' area includes: very high, high, moderate, low, and very low with 385, 253, 296, 523, and 2459 Km^2, respectively. Under scenario RCP8.5, the flood susceptibility map class area includes very high, high, moderate, low, and very low, respectively 402, 277, 339, 605, and 2309 Km^2 (Figure 9).

3.3. Validation Models and Maps

ROC curves are one of the most common methods of evaluating data mining modeling results. In this curve, the area under the ROC curve (AUC) ranges between 0.5 and 1. The closer the AUC is to 1, the more accurately the model is used to predict the phenomenon under study. To use this method, in the validation stage, 20% of the flood points were placed in front of 20% of the non-flood points, and the ROC curve was drawn. The performance of the two models used in this study, including the FDA and ANN, was evaluated using a ROC curve. The results showed that the FDA model with AUC of 0.918% compared to

the ANN model with AUC of 0.897% is more accurate in preparing the study area's flood susceptibility map (Figure 10 and Table 2).

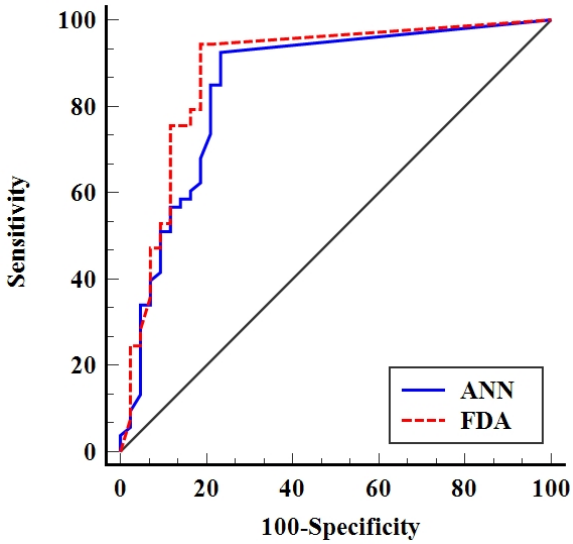

Figure 10. The validation of ANN and FDA models using ROC curves based on validation points.

Table 2. The accuracy Assessment of flood susceptibility mapping models.

Model \ Criteria	AUC	SE	%CI	Accuracy	TSS	Kappa	Bias	SR	POD
FDA	0.918	0.038	0.799 to 0.936	0.86	0.78	0.72	0.82	0.89	0.92
ANN	0.897	0.042	0.761 to 0.90	0.82	0.69	0.71	0.86	0.84	0.90

Maps prepared by two models, FDA and ANN, were also evaluated using validation points. For this purpose, the Arc Map software models' final maps were converted into fuzzy maps, and using the validation points and Extract Multi-Values to Points Tool, the values required to prepare the ROC curve were extracted. The results of the ROC curve using the validation points of the maps showed that the FDA model map under scenario RCP2.6 with a standard error (SE) of 0.03 and a confidence interval (CI) of 0.83 to 0.95 has the highest value AUC = 0.91 (Table 3). The FDA model map under scenario RCP8.5 with an SE of 0.032 and a CI of 0.81 to 0.94 had an AUC of 0.893, followed by the ANN model map under scenario RCP8.5 with a SE of 0.032 and a CI 0.81 to 0.94 had an AUC of 0.892. The ANN model map under scenario RCP2.6 had a SE of 0.035, and the CI 0.80 to 0.94 had an AUC of 0.888 (Table 3 and Figures 11 and 12).

Table 3. The accuracy assessment of flood susceptible maps of scenarios RCP2.6 and RCP8.5 using validation points.

Models \ Criteria	AUC	SE	95% CI
ANN RCP2.6	0.888	0.035	0.80 to 0.94
ANN RCP8.5	0.892	0.032	0.81 to 0.94
FDA RCP2.6	0.910	0.032	0.83 to 0.95
FDA RCP8.5	0.893	0.032	0.81 to 0.94

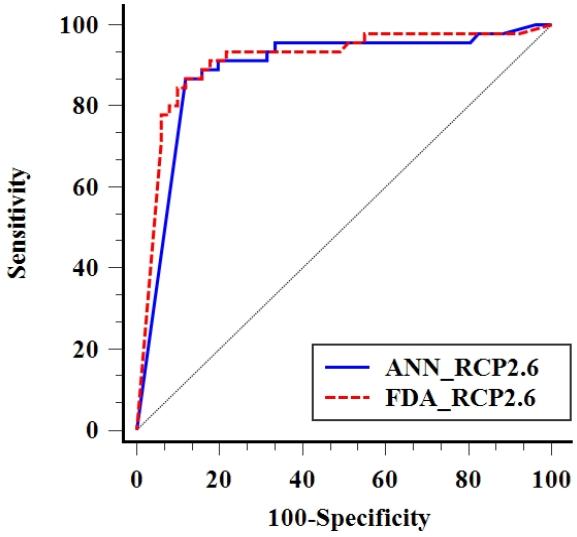

Figure 11. The validation of two flood susceptible maps (not model) under RCP2.6 scenario using the ROC curve based on validation points.

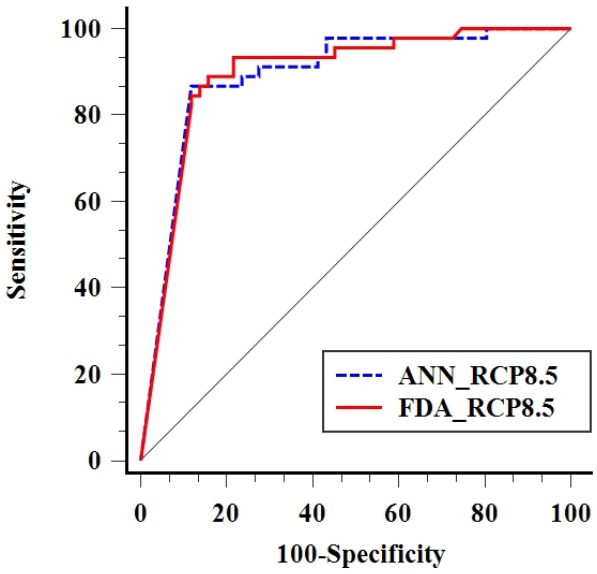

Figure 12. The validation of two flood susceptible maps (not model) under the RCP8.5 scenario using the ROC curve based on validation points.

4. Discussion

Zonation of the flood-prone area is the most crucial approach to protecting stakeholders and their assets, as area prioritization for executive plans. Therefore, flood management is an important method to prevent and reduce flood damage. For this purpose, flood susceptibility mapping has become a critical flood management method in the world. Therefore, researchers are always trying to use new methods and approaches to achieve accurate executive branch results [43,65]. Based on these cases, the current study uses a new approach to identify susceptibility and vulnerable areas to floods in the future in the Tajan River watershed using ANN and FDA data mining methods and Lars-WG climate model. Given that the north of Iran has experienced floods in different years. Hence, modeling the degree of flood susceptibility in these areas is essential.

The models used in this study have been applied in various studies on landslides [56], floods [57,66], or groundwater [67] phenomena. However, these models, along with climatic methods to flood future susceptibility maps, have not been used. Therefore, these two models' performance was evaluated under two scenarios, RCP2.6 and RCP8.5, using

the ROC curve and several other statistical criteria. Moreover, the most critical factors affecting the flood in the study area were identified.

In this study, 13 factors affecting floods were used to prepare a flood susceptibility map of the Tajan watershed. Findings showed that in both data mining models, distance from the River, altitude, slope, rainfall, and land use factors significantly impact floods in this area. Distance from the river factor is one of the most critical factors affecting floods and damage in this area. Most previous studies have been considered the most critical factor [18,68]. Due to topographic conditions, which are often mountainous and have a relatively steep slope in this area, it significantly affects the speed and volume of runoff. It causes rapid evacuation of runoff by upstream areas of the watershed and runoff accumulation in downstream and flat areas. These results are consistent with researchers' findings, such as [19,49] on topography's essential effect on floods. Rainfall and land use as two dynamic and effective factors on the watershed at different times have a significant impact on floods. In areas with dense cover such as forests, the runoff's amount and speed and the resulting damage decrease [47]. As shown in Figures 5 and 6, areas, where land use has changed from forest to agriculture or residential are also more likely to be exposed to flooding in the future. Therefore, preventing deforestation and construction along the River to reduce future damage should be a priority for policymakers.

Two data mining models, ANN and FDA, were used to predict flood probability in the Tajan watershed, Sari, Iran. The performance evaluation of the models shows that the FDA was the most efficient model. Literature review showed that the ANN model compared to some models has a higher accuracy for prediction, which contradicts the results of this study. Since ANN and FDA models have not been compared in order to prepare a flood susceptibility map, so several factors including data type and type of modeling could affect these results. Moreover, the results of evaluating the ANN and FDA model maps under two climatic scenarios RCP2.6 and RCP8.5 using the ROC curve showed that the FDA model map under scenario RCP2.6 with AUC = 0.91, compared to other climatic models and scenarios, are the most accurate for the preparation of flood susceptibility map of the study area. It is followed by the FDA model map RCP8.5 with AUC = 0.893, the ANN RCP8.5 with 0.892, and the ANN RCP2.6 with 0.888. The results of flood susceptibility classes of different models and scenarios showed that a very low class in both models and scenarios would cover the largest area in the study area, so that in the ANN model under scenarios RCP2.6 and RCP8.5 area very low class will be 1555 and 2442 Km^2, respectively. Simultaneously, in the FDA model and under scenarios RCP2.6 and RCP8.5, the area of very low classes will be 2309 and 2459 Km^2, respectively. Moreover, the minimum area of flood susceptibility classes in both models will be high class.

5. Conclusions and Future Perspectives

For the first time in this study, integrating the two data mining models of artificial neural network (ANN) and flexible discrimination analysis (FDA) with Lars-WG climate model was used for future flood susceptibility mapping in Tajan watershed, Mazandaran, Iran. Moreover, 263 flood points and 13 topographic, environmental, climatic, and hydrological factors that affected the flood were selected. They included altitude, slope, slope aspect, rainfall, land use, plan curvature, plan curvature, distance from the River, drainage density, lithology, soil, topographic wetness index (TWI), and terrain position index (TPI). Investigating factors affecting floods in the study area in both models show the more significant impact of distance factors from the River, altitude, slope, and rainfall. Evaluation of the models used to use the ROC curve showed that the FDA model under scenario RCP2.6 with AUC = 0.89 has higher accuracy in preparing the study area's flood susceptibility map. The flood susceptibility zoning map produced by both models was divided into five classes based on the natural break algorithm and based on previous research: very low, low, moderate, high, and very high. The largest area in both models and scenarios is very low class, and the lowest area is high class.

Finally, using other models and approaches of data mining and machine learning and climatic models is suggested. This increases the accuracy of flood susceptibility maps. Policymakers should prioritize flood-prone areas identified in this study and take protective and management measures if necessary, to reduce potential damage. Vulnerability and indicator factors should be identified in flood susceptible areas. Subsequently, necessary measures should be taken to strengthen those indicators and improve the resilience of watershed residents. One of the most important limitations of this research is the lack of access to some areas for field survey and determination of flooding areas. In order to model climate change in the study area, different meteorological stations have been used, which have limited data preparation and standardization of basic data.

Author Contributions: Conceptualization, M.A., H.R.M. and M.R.L.; methodology, M.A. and H.R.M.; validation, M.A. and H.R.M.; formal analysis, M.A. and H.R.M.; investigation, M.A., H.R.M. M.R.L.; resources, M.A.; data curation, M.A.; writing—original draft preparation, M.A.; writing—review and editing, M.A., H.R.M. and M.R.L.; visualization, M.A.; supervision, H.R.M. All authors have read and agreed to the published version of the manuscript.

Funding: We thank MDPI Publications and Geosciences Journal for their financial support of this article.

Institutional Review Board Statement: Not applicable.

Informed Consent Statement: Informed consent was obtained from all subjects involved in the study.

Conflicts of Interest: The authors declare no conflict of interest.

Abbreviations

ROC	receiver operating characteristic curve
AUC	area under curve
ANN	artificial neural network
FDA	flexible discrimination analysis
TPI	terrain position index
TWI	topographic wetness index
CI	confidence interval
SE	standard error
DEM	digital elevation model
TSS	true skill statistic
POD	probability of detection
SR	success ratio

References

1. IPCC. Climate Change 2013. In *The Physical Science Basis Working Group I Contribution to the Fifth Assessment Report of the Intergovernmental Panel on Climate Change Edited by 2013*; IPCC: Geneva, Switzerland, 2013.
2. Hodgkins, G.A.; Whitfield, P.H.; Burn, D.H.; Hannaford, J.; Renard, B.; Stahl, K.; Fleig, A.K.; Madsen, H.; Mediero, L.; Murphy, C.; et al. Climate-driven variability in the occurrence of major floods across North America and Europe. *J. Hydrol.* **2017**, *552*, 704–717. [CrossRef]
3. Ghasemain, B.; Asl, D.T.; Pham, B.T.; Avand, M.; Nguyen, H.D.; Janizadeh, S. Shallow landslide susceptibility mapping: A comparison between classification and regression tree and reduced error pruning tree algorithms. *Vietnam J. Earth Sci.* **2020**. [CrossRef]
4. Mitsova, D. Coupling Land Use Change Modeling with Climate Projections Catchment Near Cincinnati, Ohio. *ISPRS Int. J. Geo-Inf.* **2014**, *3*, 1256–1277. [CrossRef]
5. IPCC. *Climate Change 2017: The Physical Science Basis*; IPCC: Geneva, Switzerland, 2017.
6. Liuzzo, L.; Bono, E.; Sammartano, V.; Freni, G. Analysis of spatial and temporal rainfall trends in Sicily during the 1921–2012 period. *Appl. Clim.* **2016**, *126*, 113–129. [CrossRef]
7. Warming, G. Perceived community-based flood adaptation strategies under climate change in Nepal. *Int. J. Glob. Warm.* **2014**, *6*, 113–124.
8. Kordrostami, S.; Tao, Z.; Karim, F.; Rahman, A. Regional Flood Frequency Analysis Using an Artificial Neural Network Model. *Geoscience* **2020**, *10*, 127. [CrossRef]
9. Akter, T.; Quevauviller, P.; Eisenreich, S.J.; Vaes, G. Impacts of climate and land use changes on flood risk manage-ment for the Schijn River, Belgium. *Environ. Sci. Policy* **2018**, *89*, 163–175. [CrossRef]

10. Saber, M.; Abdrabo, K.I.; Habiba, O.M.; Kantosh, S.A.; Sumi, T. Impacts of Triple Factors on Flash Flood Vulnerability in Egypt: Urban Growth, Extreme Climate, and Mismanagement. *Geosciences* **2020**, *10*, 24. [CrossRef]
11. Kuriqi, A.; Ali, R.; Pham, Q.B.; Gambini, J.M.; Gupta, V.; Malik, A.; Linh, N.T.; Joshi, Y.; Anh, D.T.; Dong, X. Seasonality shift and streamflow flow variability trends in central India. *Acta Geophys.* **2020**, *68*, 1461–1475. [CrossRef]
12. Senent-Aparicio, J.; Jimeno-Sáez, P.; Bueno-Crespo, A.; Pérez-Sánchez, J.; Pulido-Velázquez, D. Coupling ma-chine-learning techniques with SWAT model for instantaneous peak flow prediction. *Biosyst. Eng.* **2019**, *177*, 67–77. [CrossRef]
13. Thompson, J.R.; Crawley, A.; Kingston, D.G. Future river flows and flood extent in the Upper Niger and Inner Niger Delta: GCM-related uncertainty using the CMIP5 ensemble. *Hydrol. Sci. J.* **2017**, *62*, 2239–2265. [CrossRef]
14. Ali, R.; Kuriqi, A.; Kisi, O. Human–Environment Natural Disasters Interconnection in China: A Review. *Climate* **2020**, *8*, 48. [CrossRef]
15. Bertilsson, L.; Wiklund, K.; Moura, I.; De Moura, O.; Veról, A.P.; Miguez, M.G. Urban flood resilience—A multi-criteria index to integrate flood resilience into urban planning. *J. Hydrol.* **2019**, *573*, 970–982. [CrossRef]
16. Almasi, P.; Soltani, S. Assessment of the climate change impacts on flood frequency (case study: Bazoft Basin, Iran). *Stoch. Environ. Res. Risk Assess.* **2016**, *31*, 1171–1182. [CrossRef]
17. Shahabi, H.; Jarihani, B.; Piralilou, S.T.; Chittleborough, D.; Avand, M.; Ghorbanzadeh, O. A Semi-Automated Object-Based Gully Networks Detection Using Different Machine Learning Models: A case study of Bowen Catchment, Queensland, Australia. *Sensor* **2019**, *19*, 4893. [CrossRef]
18. Yariyan, P.; Avand, M.; Abbaspour, R.A.; Haghighi, A.T.; Costache, R.; Ghorbanzadeh, O.; Janizadeh, S.; Blaschke, T. Flood susceptibility mapping using an improved analytic network process with statistical models. *Geomat. Nat. Hazards Risk* **2020**, *11*, 2282–2314. [CrossRef]
19. Talukdar, S.; Ghose, B.; Salam, R.; Mahato, S.; Pham, Q.B.; Linh, N.T.T.; Avand, M. Flood susceptibility modeling in Teesta River basin, Bang-ladesh using novel ensembles of bagging algorithms. *Stoch. Environ. Res. Risk Assess.* **2020**, *34*, 2277–2300. [CrossRef]
20. Abdelkarim, A.; Al-Alola, S.S.; Alogayell, H.M.; Mohamed, S.A.; Alkadi, I.I.; Youssef, I.Y. Mapping of GIS-Flood Hazard Using the Geomorphometric-Hazard Model: Case Study of the Al-Shamal Train Pathway in the City of Qurayyat, Kingdom of Saudi Arabia. *Geosciences* **2020**, *10*, 333. [CrossRef]
21. Avand, M.; Janizadeh, S.; Tien Bui, D.; Pham, V.H.; Ngo, P.T.; Nhu, V.H. A tree-based intelligence ensemble approach for spatial prediction of potential groundwater. *Int. J. Digit. Earth* **2020**, 1–22. [CrossRef]
22. Garner, A.J.; Mann, M.E.; Emanuel, K.A.; Kopp, R.E.; Lin, N.; Alley, R.B.; Horton, B.P.; DeConto, R.M.; Donnelly, J.P.; Pollard, D. Impact of climate change on New York City's coastal flood hazard: Increasing flood heights from the preindustrial to 2300 CE. *Proc. Natl. Acad. Sci. USA* **2017**, *114*, 11861–11866. [CrossRef]
23. Hirabayashi, Y.; Mahendran, R.; Koirala, S.; Konoshima, L.; Yamazaki, D.; Watanabe, S.; Kim, H.; Kanae, S. Global flood risk under climate change. *Nat. Clim. Chang.* **2013**, *3*, 816–821. [CrossRef]
24. Dobler, C.; Bürger, G.; Stötter, J. Assessment of climate change impacts on flood hazard potential in the Al-pine Lech watershed. *J. Hydrol.* **2012**, *460*, 29–39. [CrossRef]
25. Dankers, R.; Feyen, L. Flood hazard in Europe in an ensemble of regional climate scenarios. *J. Geophys. Res. Atmos.* **2009**, *114*, 114. [CrossRef]
26. Islam, A.R.M.T.; Talukdar, S.; Mahato, S.; Kundu, S.; Eibek, K.U.; Pham, Q.B.; Kuriqi, A.; Linh, N.T. Flood susceptibility modelling using advanced ensemble machine learning models. *Geosci. Front.* **2020**. [CrossRef]
27. Mendizabal, M.; Sepúlveda, J.; Torp, P. Climate change impacts on flood events and its consequences on hu-man in Deba River. *Int. J. Environ. Res.* **2014**, *8*, 221–230.
28. Roy, P.; Pal, S.C.; Chakrabortty, R.; Chowdhuri, I.; Malik, S.; Das, B. Threats of climate and land use change on future flood susceptibility. *J. Clean. Prod.* **2020**, *272*, 122757. [CrossRef]
29. Xie, H.; Hu, X.J. Time-Series Data Mining of Minimum Design Height for River Bridge Deck Using Seasonal Trend Decomposition. *Phys. Conf. Ser.* **2019**, *1284*, 012042. [CrossRef]
30. Jung, C.; Lee, J.-W.; Lee, Y.; Kim, S.-J. Quantification of Stream Drying Phenomena Using Grid-Based Hydrological Modeling via Long-Term Data Mining throughout South Korea including Ungauged Areas. *Water* **2019**, *11*, 477. [CrossRef]
31. Salih, S.Q.; Sharafati, A.; Khosravi, K.; Faris, H. River suspended sediment load prediction based on riv-er discharge information: Application of newly developed data mining models. *Hydrol. Sci. J.* **2020**, *65*, 624–637. [CrossRef]
32. Moradi, H.R.; Avand, M.T.; Janizadeh, S. *Spatial Modeling in GIS and R for Earth and Environmental Sciences*; Elsevier: Amsterdam, The Netherlands, 2019; pp. 259–275.
33. Hassani, H.; Huang, X.; Silva, E.S. Big Data and Climate Change. *Big Data Cogn. Comput.* **2019**, *3*, 12. [CrossRef]
34. Khosravi, K.; Daggupati, P.; Alami, M.T.; Awadh, S.M.; Ghareb, M.I.; Panahi, M.; Pham, B.T.; Rezaie, F.; Qi, C.; Yaseen, Z.M. Meteorological data mining and hybrid data-intelligence models for reference evaporation simulation: A case study in Iraq. *Comput. Electron. Agric.* **2019**, *167*, 105041. [CrossRef]
35. Rajaei, F.; Esmaili, A.; Abdolrassoul, S. Surface drainage nitrate loading estimate from agriculture fields and its relationship with landscape metrics in Tajan watershed. *Paddy Water Environ.* **2017**, *15*, 541–552. [CrossRef]
36. Bui, D.T.; Tsangaratos, P.; Ngo, P.T.T.; Pham, T.D.; Pham, B.T. Flash flood susceptibility modeling using an optimized fuzzy rule based feature selection technique and tree based ensemble methods. *Sci. Total Environ.* **2019**, *668*, 1038–1054. [CrossRef] [PubMed]

37. Pham, B.T.; Avand, M.; Janizadeh, S.; Van Phong, T.; Al-Ansari, N.; Ho, L.S.; Das, S.; Van Le, H.; Amini, A.; Bozchaloei, S.K.; et al. GIS Based Hybrid Computational Approaches for Flash Flood Susceptibility Assessment. *Water* **2020**, *12*, 683. [CrossRef]
38. Costache, R.; Pham, Q.B.; Sharifi, E.; Linh, N.T.T.; Abba, S.I.; Vojtek, M.; Vojteková, J.; Nhi, P.T.T.; Khoi, D.N. Flash-Flood Susceptibility Assessment Using Multi-Criteria Decision Making and Machine Learning Supported by Remote Sensing and GIS Techniques. *Remote Sens.* **2019**, *12*, 106. [CrossRef]
39. Tehrany, M.S.; Pradhan, B.; Jebur, M.N. Flood susceptibility mapping using a novel ensemble weights-of-evidence and support vector machine models in GIS. *J. Hydrol.* **2014**, *512*, 332–343. [CrossRef]
40. Chapi, K.; Singh, V.P.; Shirzadi, A.; Shahabi, H.; Bui, D.T.; Pham, B.T.; Khosravi, K. A novel hybrid artificial intelligence approach for flood susceptibility assessment. *Environ. Model. Softw.* **2017**, *95*, 229–245. [CrossRef]
41. Al-Juaidi, A.E.M.; Nassar, A.M.; Al-Juaidi, O.E.M. Evaluation of flood susceptibility mapping using logistic regression and GIS conditioning factors. *Arab. J. Geosci.* **2018**, *11*, 765. [CrossRef]
42. Lee, M.-J.; Kang, J.-E.; Jeon, S. Application of frequency ratio model and validation for predictive flooded area susceptibility mapping using GIS. In Proceedings of the 2012 IEEE International Geoscience and Remote Sensing Symposium, Munich, Germany, 22–27 July 2012.
43. Zhao, G.; Pang, B.; Xu, Z.; Peng, D.; Xu, L. Assessment of urban flood susceptibility using semi-supervised machine learning model. *Sci. Total Environ.* **2019**, *659*, 940–949. [CrossRef]
44. Pradhan, B. Journal of Spatial Hydrology Biswajeet Pradhan. *J. Spat. Hydrol.* **2009**, *9*, 1–18.
45. Pradhan, B.; Youssef, A.M. A100-year maximum flood susceptibility mapping using integrated hydrological and hydrodynamic models: Kelantan River Corridor, Malaysia. *J. Flood Risk Manag.* **2011**, *4*, 189–202. [CrossRef]
46. Nachappa, T.G.; Piralilou, S.T.; Gholamnia, K.; Ghorbanzadeh, O.; Rahmati, O.; Blaschke, T. Flood susceptibility mapping with machine learning, multi-criteria decision analysis and ensemble using Dempster Shafer Theory. *J. Hydrol.* **2020**, *590*, 125275. [CrossRef]
47. Costache, R.; Popa, M.C.; Bui, D.T.; Diaconu, D.C.; Ciubotaru, N.; Minea, G.; Pham, Q.B. Spatial predicting of flood potential areas using novel hybridizations of fuzzy decision-making, bivariate statistics, and machine learning. *J. Hydrol.* **2020**, *585*, 124808. [CrossRef]
48. Rahmati, O.; Pourghasemi, H.R.; Zeinivand, H. Flood susceptibility mapping using frequency ratio and weights-of-evidence models in the Golastan Province, Iran. *Geocarto Int.* **2016**, *31*, 42–70. [CrossRef]
49. Costache, R. Flood Susceptibility Assessment by Using Bivariate Statistics and Machine Learning Models-A Useful Tool for Flood Risk Management. *Water Resour. Manag.* **2019**, 1–18. [CrossRef]
50. Costache, R.; Pham, Q.B.; Avand, M.; Linh, N.T.T.; Vojtek, M.; Vojteková, J.; Dung, T.D. Novel hybrid models between bivariate statistics, ar-tificial neural networks and boosting algorithms for flood susceptibility assessment. *J. Environ. Manag.* **2020**, *265*, 110485. [CrossRef]
51. Hastie, T.; Tibshirani, R.; Friedman, J. *The Elements of Statistical Learning: Data Mining, Inference, and Prediction*; Springer: Berlin/Heidelberg, Germany, 2009.
52. Ashrafzadeh, M.R.; Naghipour, A.A.; Haidarian, M.; Khorozyan, I. Modeling the response of an endangered flagship predator to climate change in Iran. *Mammal Res.* **2018**, *64*, 39–51. [CrossRef]
53. Hastie, T.; Tibshirani, R.; Buja, A. *Flexible Discriminant and Mixture Models*; Stanford University: Stanford, CA, USA, 1995.
54. Roth, V.; Steinhage, V. Nonlinear discriminant analysis using kernel functions. *Adv. Neural Inf. Process. Syst.* **1999**, *12*, 568–574.
55. Dawson, C.W.; Abrahart, R.J.; Shamseldin, A.Y.; Wilby, R.L. Flood estimation at ungauged sites using artifi-cial neural networks. *J. Hydrol.* **2006**, *319*, 391–409. [CrossRef]
56. Pradhan, B.; Lee, S.; Buchroithner, M.F. A GIS-based back-propagation neural network model and its cross-application and validation for landslide susceptibility analyses. *Comput. Environ. Urban Syst.* **2010**, *34*, 216–235. [CrossRef]
57. Mukerji, A.; Chatterjee, C.; Raghuwanshi, N.S. Flood Forecasting Using ANN, Neuro-Fuzzy, and Neuro-GA Models. *J. Hydrol. Eng.* **2009**, *14*, 647–652. [CrossRef]
58. Pham, B.T.; Jaafari, A.; Avand, M.; Al-Ansari, N.; Du, T.D.; Yen, H.P.H.; Van Phong, T.; Nguyen, H.D.; Van Le, H.; Mafi-Gholami, D.; et al. Performance Evaluation of Machine Learning Methods for Forest Fire Modeling and Prediction. *Symmetry* **2020**, *12*, 1022. [CrossRef]
59. Lei, X.; Chen, W.; Avand, M.; Janizadeh, S.; Kariminejad, N.; Shahabi, H.; Costache, R.; Shahabi, H.; Shirzadi, A.; Mosavi, A. GIS-Based Machine Learning Algorithms for Gully Erosion Susceptibility Mapping in a Semi-Arid Region of Iran. *Remote Sens.* **2020**, *12*, 2478. [CrossRef]
60. Pham, B.T.; Van Phong, T.; Avand, M.; Al-Ansari, N.; Singh, S.K.; Van Le, H.; Prakash, I. Improving Voting Feature Intervals for Spatial Prediction of Landslides. *Math. Probl. Eng.* **2020**, *2020*, 4310791. [CrossRef]
61. Yousefi, S.; Avand, M.; Yariyan, P.; Pourghasemi, H.R.; Keesstra, S.; Tavangar, S.; Tabibian, S. A novel GIS-based ensemble technique for rangeland downward trend mapping as an ecological indicator change. *Ecol. Indic.* **2020**, *117*, 106591. [CrossRef]
62. Avand, M.; Moradi, H.; Ramazanzadeh, M. Using machine learning models, remote sensing, and GIS to investigate the effects of changing climates and land uses on flood probability. *J. Hydrol.* **2020**, 125663. [CrossRef]
63. Avand, M.; Janizadeh, S.; Naghibi, S.A.; Pourghasemi, H.R. A Comparative Assessment of Random Forest and k-Nearest Neighbor Classifiers for Gully Erosion Susceptibility Mapping. *Water* **2019**, *11*, 2076. [CrossRef]

64. Costache, R.; Ţincu, R.; Elkhrachy, I.; Pham, Q.B.; Popa, M.C.; Diaconu, D.C.; Bui, D.T. New neural fuzzy-based machine learning ensem-ble for enhancing the prediction accuracy of flood susceptibility mapping. *Hydrol. Sci. J.* **2020**, *65*, 2816–2837. [CrossRef]
65. Ahmadlou, M.; Karimi, M.; Alizadeh, S.; Shirzadi, A.; Parvinnejhad, D.; Shahabi, H.; Panahi, M. Flood susceptibility assessment using integration of adaptive network-based fuzzy inference system (ANFIS) and biogeography-based optimization (BBO) and BAT algo-rithms (BA). *Geocarto Int.* **2019**, *34*, 1252–1272. [CrossRef]
66. Shafizadeh-Moghadam, H.; Valavi, R.; Shahabi, H.; Chapi, K.; Shirzadi, A. Novel forecasting approaches us-ing combination of machine learning and statistical models for flood susceptibility mapping. *J. Environ. Manag.* **2018**, *217*, 1–11. [CrossRef]
67. Nourani, V.; Mousavi, S. Spatiotemporal groundwater level modeling using hybrid artificial intelligence-meshless method. *J. Hydrol.* **2016**, *536*, 10–25. [CrossRef]
68. Tehrany, M.S.; Pradhan, B.; Jebur, M.N. Flood susceptibility analysis and its verification using a novel ensem-ble support vector machine and frequency ratio method. *Stoch. Environ. Res. Risk Assess.* **2015**, *29*, 1149–1165. [CrossRef]